SI Appendix

Longitudinal multiparameter assay of lymphocyte interactions from onset by microfluidic cell pairing and culture

Burak Dura[a, b, c, 1], Mariah M. Servos[d], Rachel M. Barry[e], Hidde L. Ploegh[f, g], Stephanie K. Dougan[d, f, h], Joel Voldman[a, b, c, 1]

[a] Research Laboratory of Electronics, Massachusetts Institute of Technology (MIT), Cambridge, MA, 02139, USA.
[b] Electrical Engineering and Computer Science Department, Massachusetts Institute of Technology, Cambridge, MA, 02139, USA.
[c] Microsystems Technology Laboratory, Massachusetts Institute of Technology, Cambridge, MA, 02139, USA.
[d] Department of Cancer Immunology and AIDS, Dana-Farber Cancer Institute, Boston, MA, 02215
[e] David H. Koch Institute for Integrative Cancer Research, Massachusetts Institute of Technology, Cambridge, MA 02139
[f] Whitehead Institute for Biomedical Research, Massachusetts Institute of Technology, Cambridge, MA, 02142, USA.
[g] Department of Biology, Massachusetts Institute of Technology, Cambridge, MA, 02142, USA.
[h] Division of Immunology, Harvard Medical School, Boston, MA, 02115, USA
[1] Corresponding authors: B.D. (dura@mit.edu), J.V. (voldman@mit.edu)

Table of Contents

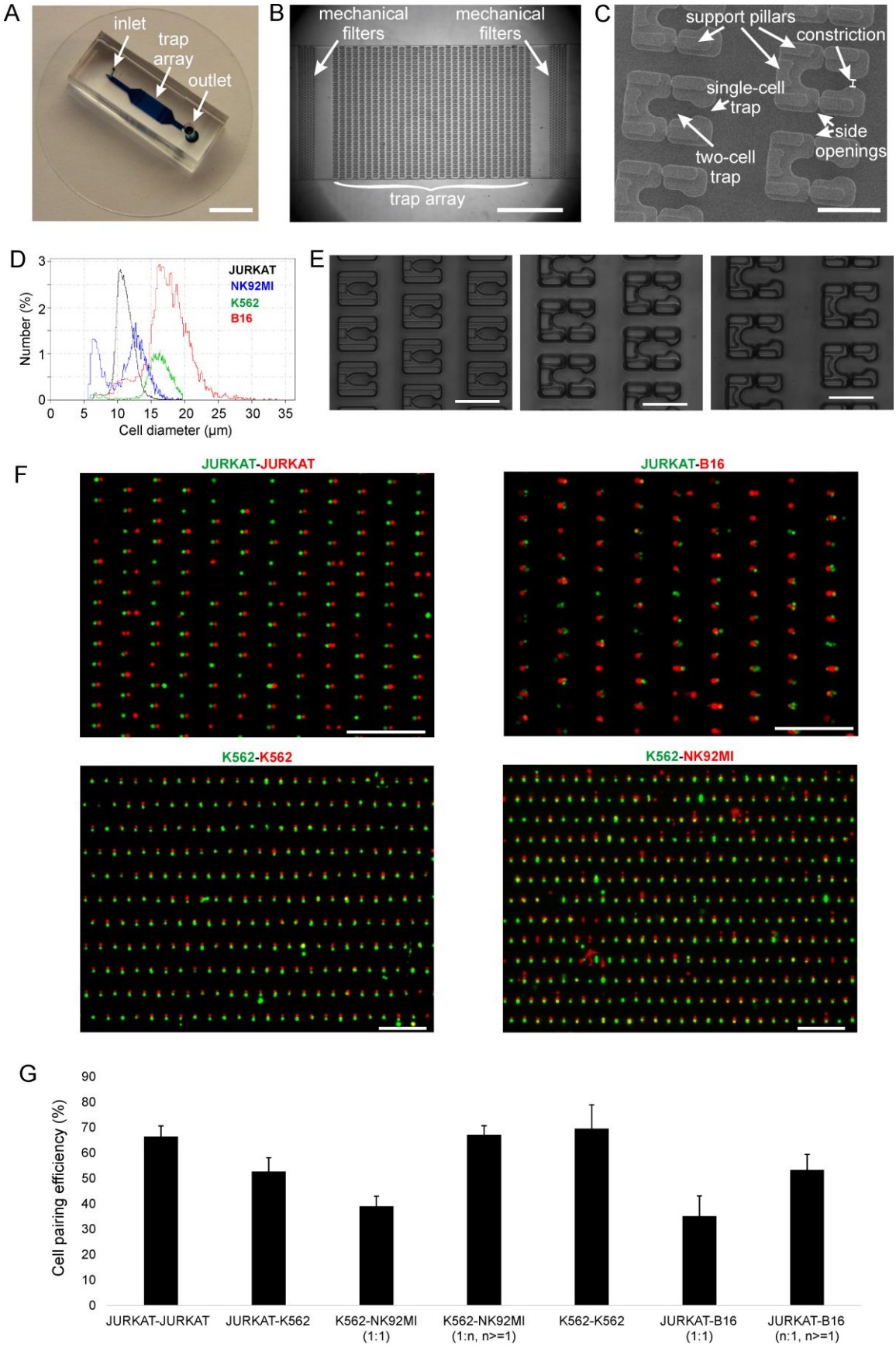
A
inlet
trap array
outlet
B
mechanical filters
mechanical filters
trap array
C
support pillars
constriction
single-cell trap
side openings
two-cell trap
D
JURKAT
NK92MI
K562
B16
Number (%)
Cell diameter (μm)
E
F
JURKAT-JURKAT
JURKAT-B16
K562-K562
K562-NK92MI
G
Cell pairing efficiency (%)
JURKAT-JURKAT
JURKAT-K562
K562-NK92MI (1:1)
K562-NK92MI (1:n, n>=1)
K562-K562
JURKAT-B16 (1:1)
JURKAT-B16 (n:1, n>=1)

Figure S1. Microfluidic cell pairing and culture platform. (A) Image of the device. Channels and trap array are in blue. (B) Image of the entire trap array which consists of ~1000 traps in 2×3 mm^2 area. Mechanical filters help break any cell aggregates to ensure single-cell loading while minimizing clogging. (C) Scanning electron micrograph image of the cell trap structure, detailing the single-cell trap, two-cell trap, constriction and support pillars. (D) Size distribution of cell types used to characterize cell pairing devices in this study. Cell size distribution covers a wide range from 9 μm to 25 μm in diameter. Cell size measurements were acquired using a Coulter counter (Beckman Coulter Z2). (E) Representative images of devices fabricated for accommodating various cell sizes. Note that side gaps are omitted in the smaller devices. (F) Representative images of cell pairing within microfluidic devices using various cell types. (G) Quantification of cell pairing efficiencies (n >= 3 for each case). For pairing NK92MI-K562 and Jurkat-B16 cells, efficiencies are lower primarily due to cell aggregates in NK cell case (mostly doublets and triplets formed by NK cells that still persisted after cell preparation procedures) and capturing >1 jurkat cells in single cell traps in large devices. These are also reflected in the re-calculated efficiencies including the traps occupied with one partner cell and more than one NK or jurkat cells (~50-70%), which was similar to efficiencies obtained with other cell pairs. Scale bars: (A) 5mm, (B) 1 mm, (C) 50 μm, (D) 50 μm, (F) 200 μm.

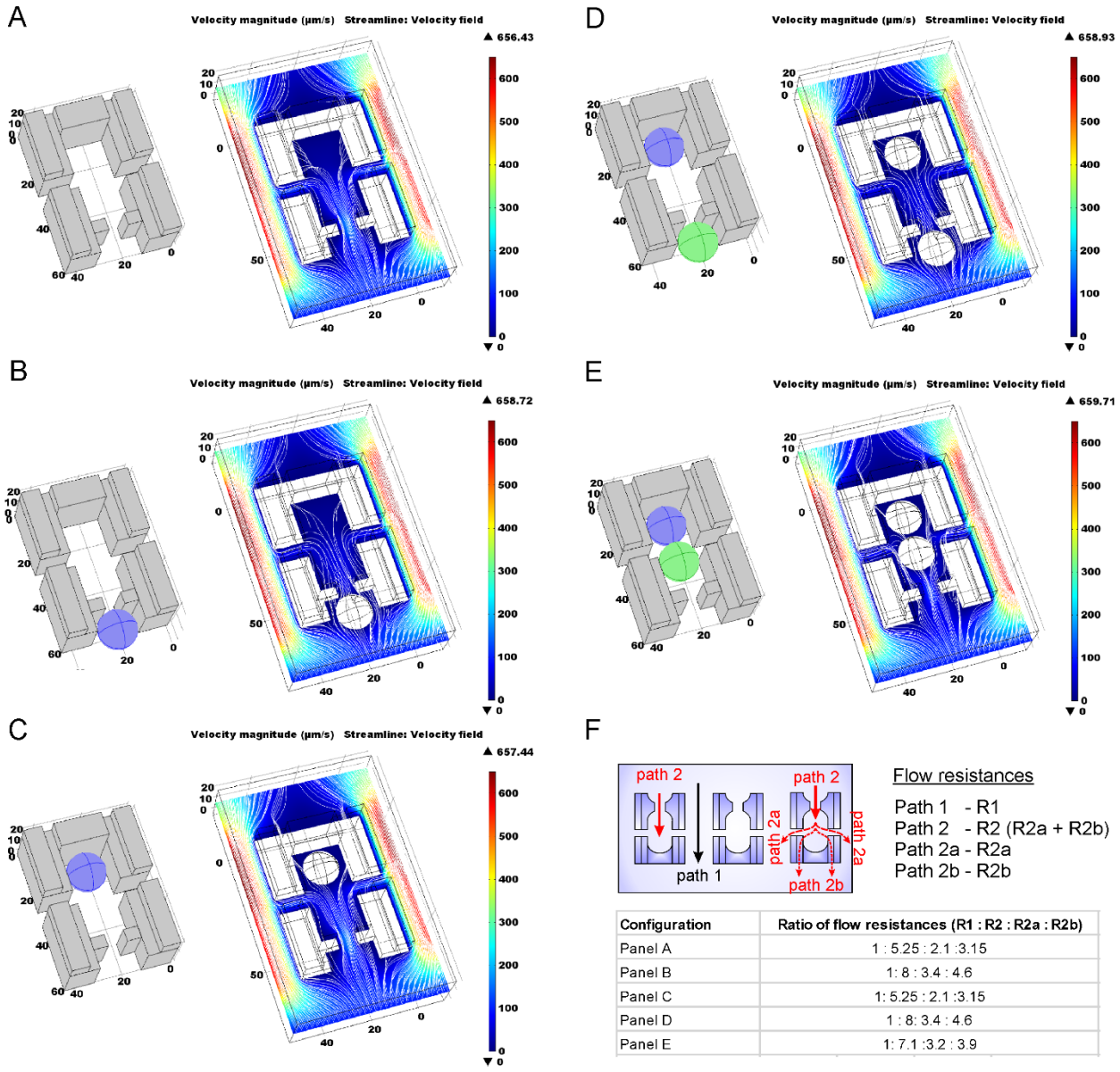

Configuration	Ratio of flow resistances (R1 : R2 : R2a : R2b)
Panel A	1 : 5.25 : 2.1 :3.15
Panel B	1: 8 : 3.4 : 4.6
Panel C	1: 5.25 : 2.1 :3.15
Panel D	1 : 8: 3.4 : 4.6
Panel E	1: 7.1 :3.2 : 3.9

Figure S2. Fluidic model of capture cups. Simulated flow profiles around the capture cups: (A) empty trap, (B) first cell is captured in the single-cell trap, (C) first cell is transferred into two-cell trap, (D) second cell is captured in the single-cell trap, (D) second cell is transferred into two-cell trap. (F) Flow resistance ratios of depicted fluidic paths in configurations shown in panels A through E.

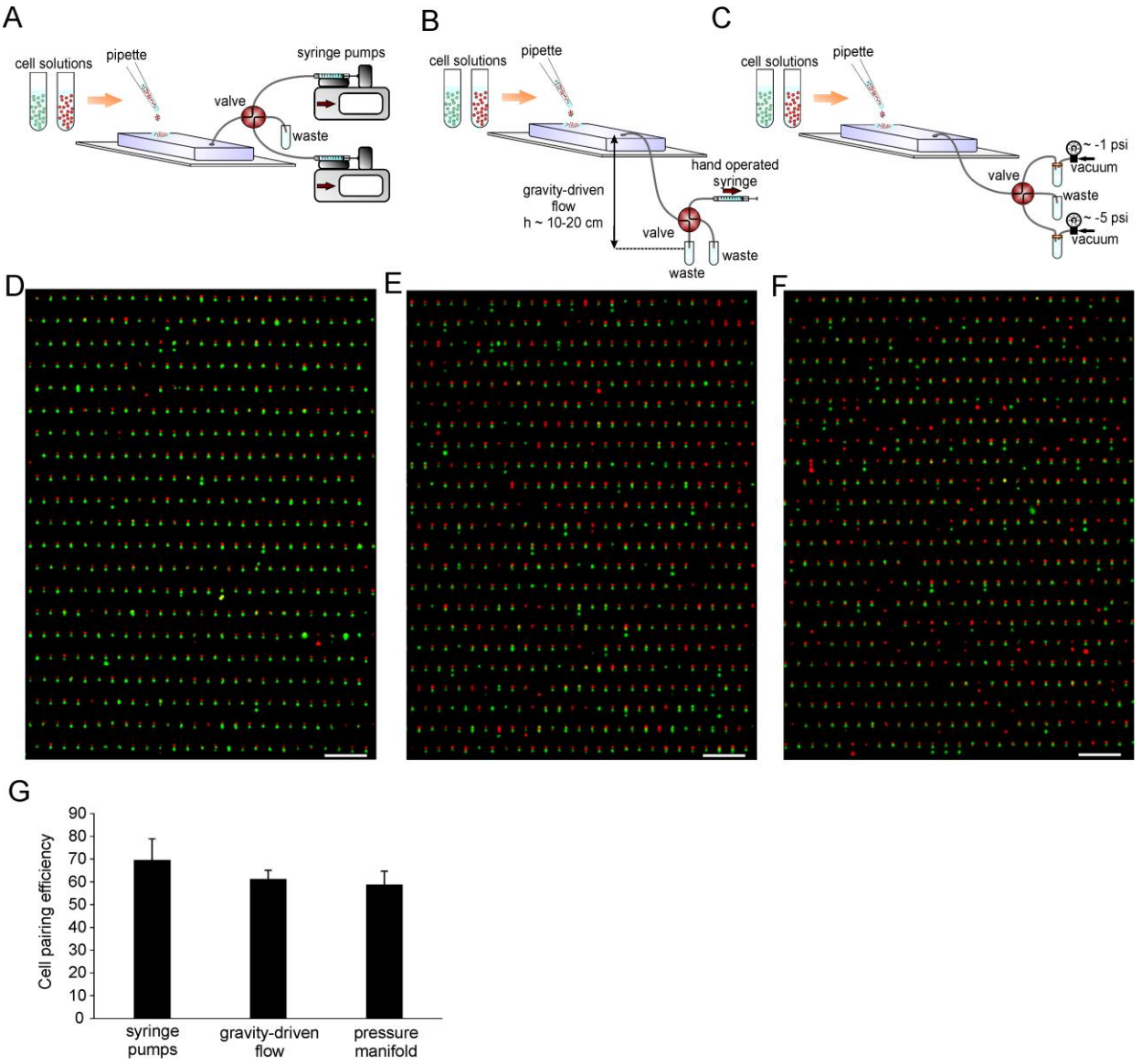

Figure S3. Alternative cell loading protocols. (A) The conventional cell loading protocol utilizes two syringe pumps running at different flow rates, one at low flow rate for capturing and infusing cells, the other at high flow rate to squeeze cells into the traps. (B, C) Additionally, device operation is also compatible with two alternative manual loading procedures. The first alternative approach uses manually operated syringe with gravity-driven flow (B). The flow rate can be controlled adjusting the height of the pressure head. While the gravity-driven flow is used to infuse and capture cells, the cells are squeezed into the traps by a brief increase in the pressure difference induced via the manually operated syringe. (C) The second alternative approach utilizes a manually controlled pressure manifold connected to a vacuum line. Two negative pressure regulators provide flow rates, one for infusing and capturing cells (~ - 1-1.5 psi) and the other for squeezing cells into the traps with a temporary increase in pressure (~ - 5-10 psi). A manually operated valve is used to switch flow between the two different pressure levels. (D-F) Representative images depicting cell pairing with fluorescently stained K562 cells using the (D) syringe pumps, (E) gravity-driven flow and manually operated syringe pump, and (F) manually operated pressure manifold. (G) Cell pairing efficiencies for K562 cells using different loading

protocols (n=5 using syringe pumps, n=3 using gravity-driven flow and pressure manifold). With optimized loading parameters, similar loading efficiencies can be obtained with all three approaches. In all approaches, devices can be disconnected from the fluidic hardware following pairing to transfer devices in between incubator and microscopy setup.

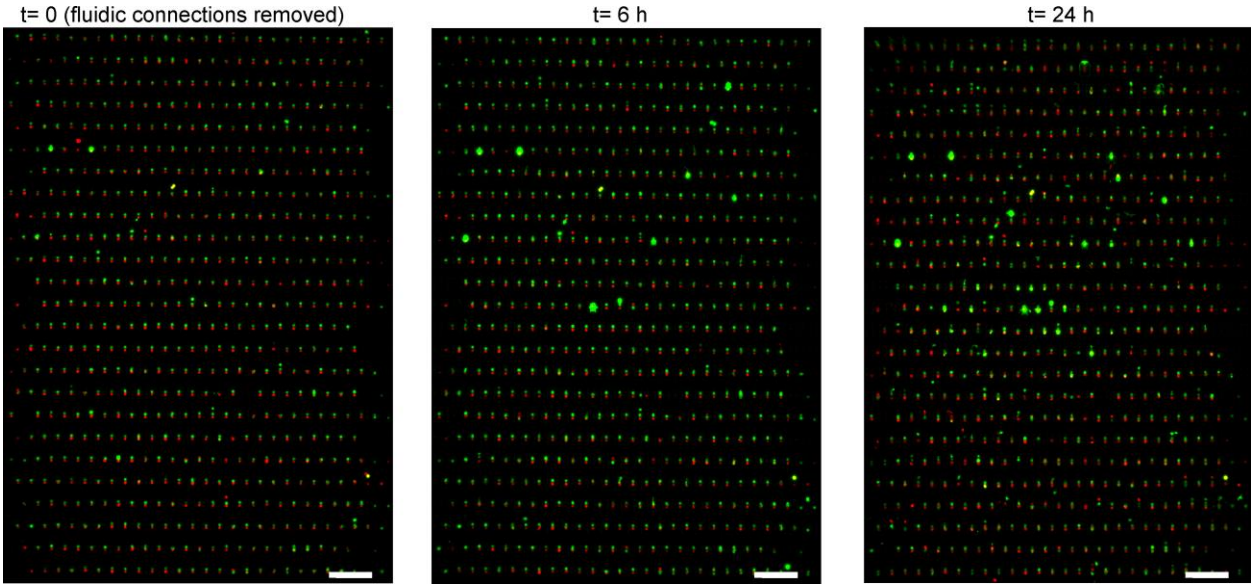

Figure S4. Longitudinal imaging and one-day culture of cell pairs (K562 cells) within their traps. Images were acquired at t=0 (right after removing fluidic connections), t=6 h and t=24 h to demonstrate preservation of cell pairing and cell viability. Cells were cultured in media with SYTOX green nuclear stain to label dead cells. Scale bars 200 μm. Representative of 3 independent experiments.

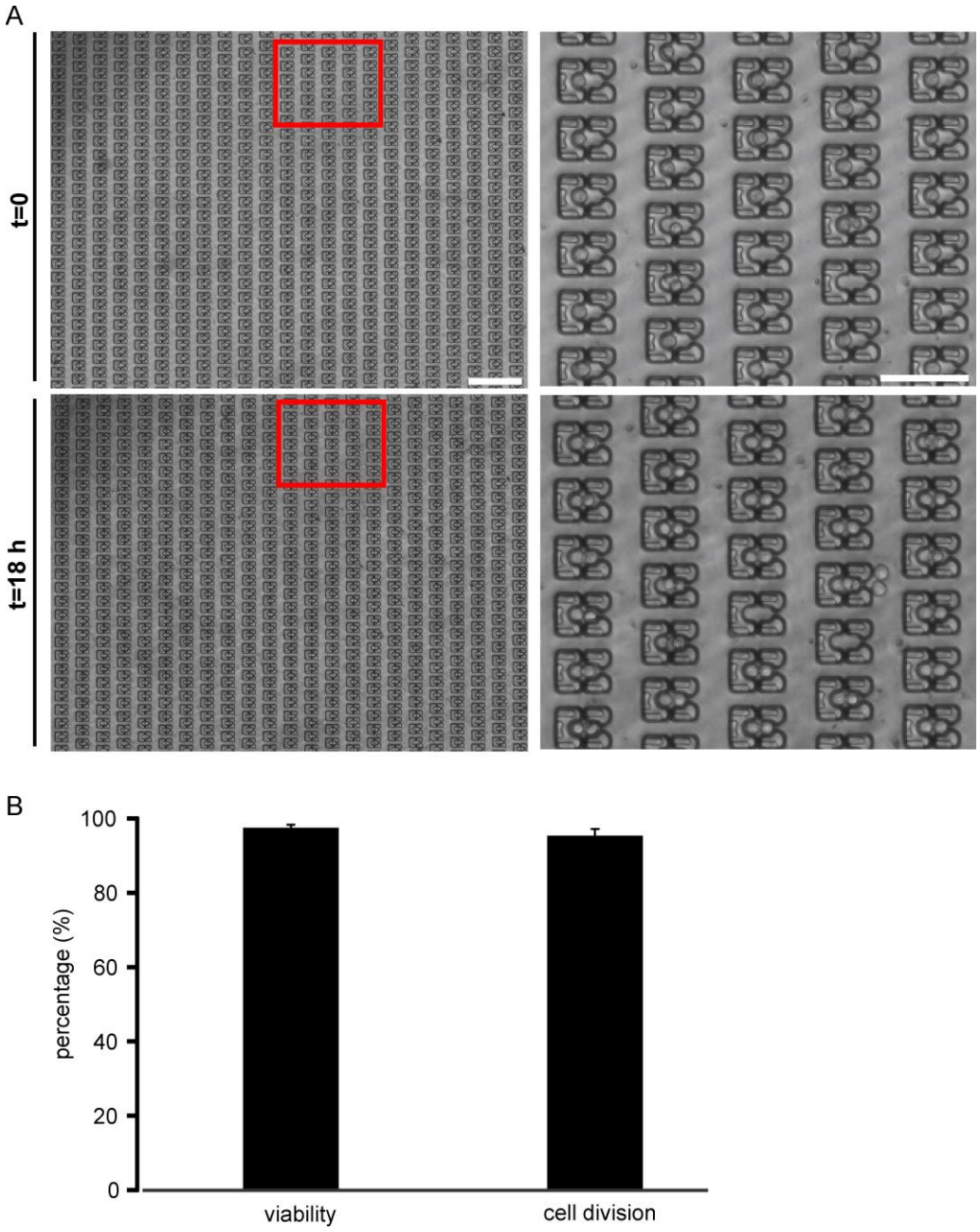

Figure S5. Cell proliferation on-chip. (A) Image of single K562 cells loaded into the traps at t=0 (upper panels). Magnified image of the inset (depicted with red rectangle in the left-most image) shown to the right. Image of the same field of view after 18 h on-chip culture is shown in bottom panels with magnified image of the inset shown to the right. Cell divisions were apparent by the presence of cell doubles in traps that were occupied with single cells at t=0. Doubling rates were ~ 18 h matching that of bulk cultures (~18-24 h). Scale bars: 250 μm (left) and 100 μm (right). (B) Quantification of cell viability and cell division over K562 cells during 24 h on-chip culture. Results are from 3 independent experiments.

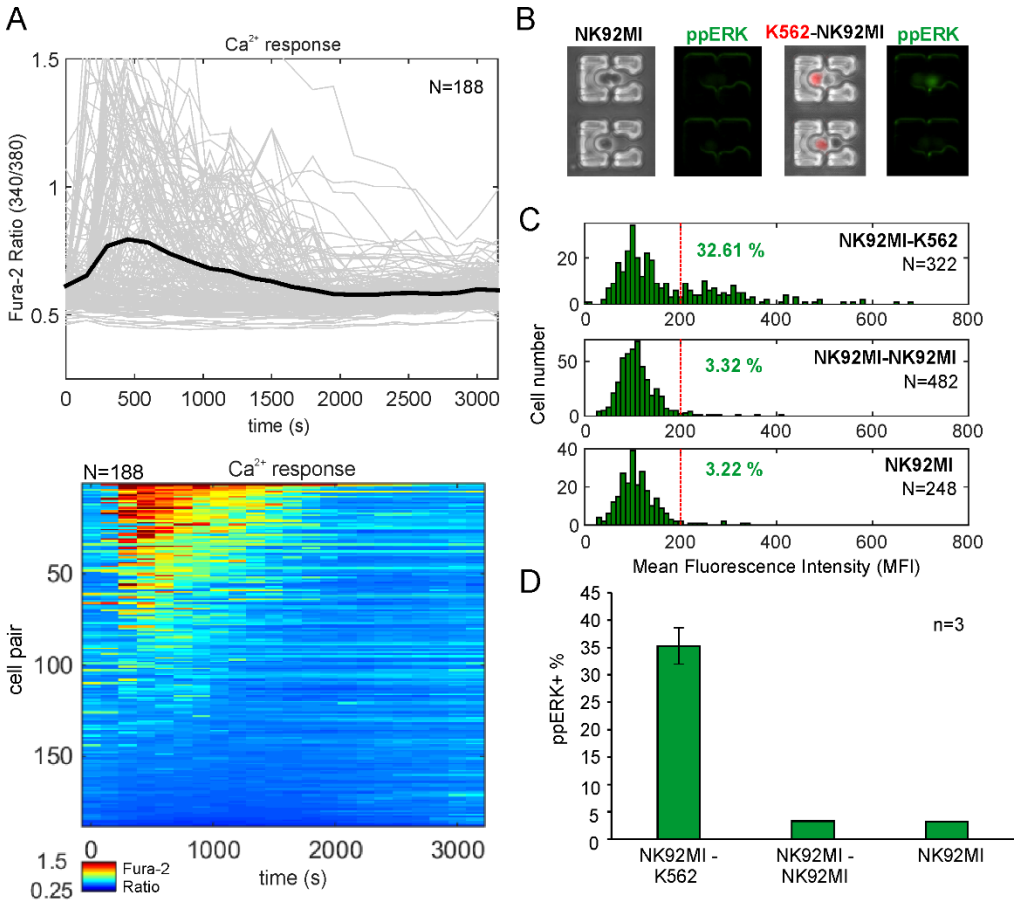

Figure S6. Measurement of early activation dynamics and molecular events. (A) Ca^{2+} response dynamics (Fura-2) of NK92MI cells upon pairing with K562 cells, recorded using ratiometric imaging. Time-plots shown in the upper panel. t=0 marks the initiation of interaction. Each grey trace represents the response of a single NK92MI cell. Black trace represents the average response. Corresponding Ca^{2+} heat maps are shown in the bottom panel (in 'jet' colormap), each row corresponding to the calcium response (Fura-2 ratio) of an individual NK92MI cell. Responses are shown in descending order based on integrated Ca^{2+} response. N represents the number of cells analyzed. Representative of 6 independent experiments. (B) Measurement of ERK phosphorylation (ppERK) of NK92MI cells (unstained) following pairing with K562 cells (Cell Tracker Orange), 10 min after initiation of interactions. Controls include NK92MI cells alone or within pairs. ppERK signals were detected using FITC conjugated antibodies. (C) ppERK measurements over NK92MI cells paired with K562 cells (upper panel), over NK92MI pairs (middle panel) and over single NK92MI cells. N represents the number of cells analyzed for each condition. Red dotted lines represent the threshold for ppERK positive events. Results are representative of 3 independent experiments. (D) Percentage of ppERK positive events for conditions in shown in (c). Results are from 3 independent experiments.

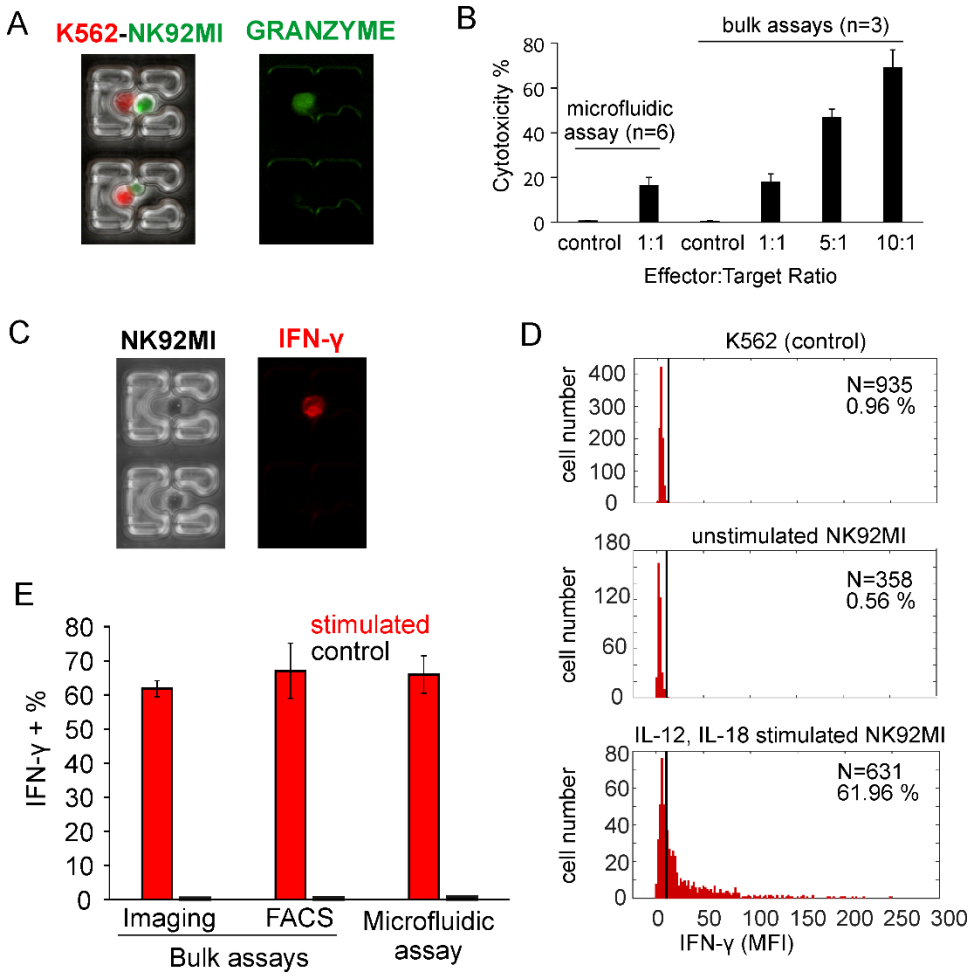

Figure S7. Measurement of functional responses of NK92MI cells. (A, B) Measurement of cytotoxicity of NK92MI cells (Fura-2 stained) paired with K562 cells (Cell Tracker Orange). (A) On-chip cytotoxicity was measured directly on K562 cells using a fluorogenic granzyme substrate (FITC, green). (B) Comparison of NK92MI cell cytotoxicity response obtained using microfluidic assay (using fluorogenic granzyme substrate as readout) and conventional bulk assays (using Sytox Green viability stain as readout). Microfluidic assays results are from 6 independent experiments. Bulk assay results are from 3 independent experiments. (C-E) Measurement of IFNg production using on-chip intracellular staining. (C) Cytokine primed (IL-12, IL-18) NK92MI cells loaded into the traps as single cells, incubated with BD Golgi Plug for 6 h, and then fixed and permeabilized for intracellular IFNg detection. IFNg expression shown in red. (D) Comparison of IFN-γ production between unstimulated and cytokine primed (IL-12, IL-18) NK92MI cells. K562 cells are used as a control for thresholding IFN-γ positive events (left panel). Unstimulated NK92 cells did not display noticeable endogeneous IFN-γ production (middle panel). Cytokine stimulation induced robust INF-γ production from NK92MI cells (right panel). N represents the number of cells analyzed for each condition. Percentages of IFN-γ producing cells shown in each figure. Representative of two independent experiments. (E) Comparison of percentages of IFNg producing cells using microfluidic assay and bulk assays. Similar results obtained via analogous bulk assays that were analyzed either using fluorescence microscopy or FACS. Unstimulated NK92MI cells were used as control. Results are from 3 independent experiments.

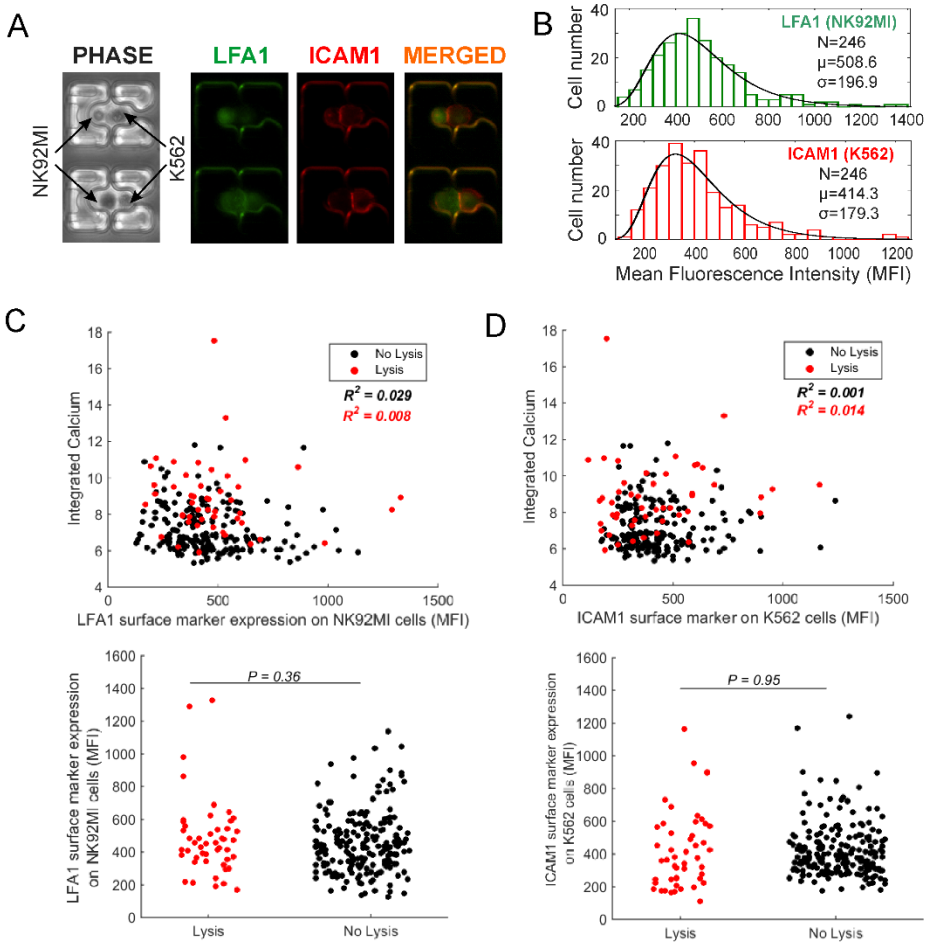

Figure S8: Measurement of surface molecule expression of cell pairs. (A, B) Measurement of cell surface marker expression using on-chip antibody staining and imaging. (A) Images depict individual and merged channels. Arrows point to NK92MI and K562 cells in phase contrast images. LFA1 expression in green, ICAM1 expression in red. (B) Representative histogram plots showing relative LFA1 expression on NK92MI cells and relative ICAM1 expression on K562 cells (below panels). N represent number of cells analyzed, μ represent mean relative expression level, and σ represent the standard deviation. (C) Correlation analysis between LFA1 marker and integrated calcium levels (upper panel) and cytotoxicity status (lower panel) of NK92MI cells. Coefficient of determinants (R^2) shown for linear correlation. (D) Correlation analysis between ICAM1 marker on K562 cells and integrated calcium levels (upper panel) and cytotoxicity status (lower panel) of NK92MI cells. Coefficient of determinants (R^2) shown for linear correlation. Representative result of 3 independent experiments.

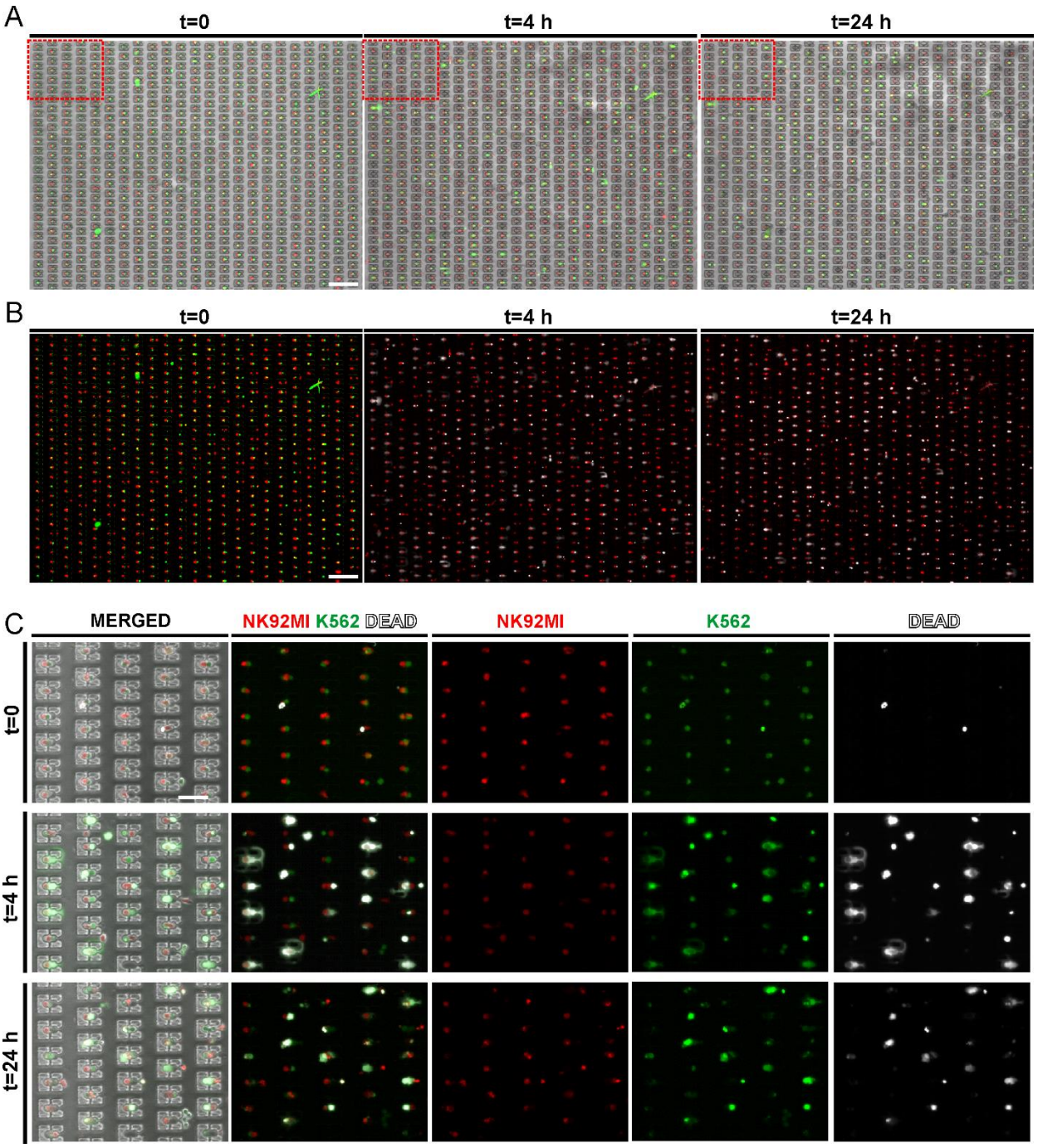

Figure S9. One-day on-chip culture of cytokine (IL-12, IL-18) primed NK92MI cells (Cell Tracker Orange) paired with K562 cells (Cell Tracker Green). (**a**) Overlaid phase contrast and fluorescence images over entire array at t=0, t=4 h and t=24 h. (**b**) Overlaid fluorescence images (same field of view as in (**a**)) at t=0, t=4 h and t=24 h. NK92MI cells in red, K562 cells in green, dead cells in white. Cytolysis of K562 cells was evident at t=4, with ~60% cytotoxicity (highest observed in our experiments) quantified over 1:1 target:effector ratio. (**c**) Magnified images of insets depicted in (**a**), displayed in overlaid and individual channels at t=0, t=4 h and t=24 h. Viability of NK92MI cells is >99% at t=4 h, and 83±3 % at t=24 h. Results are representative of 3 independent experiments.

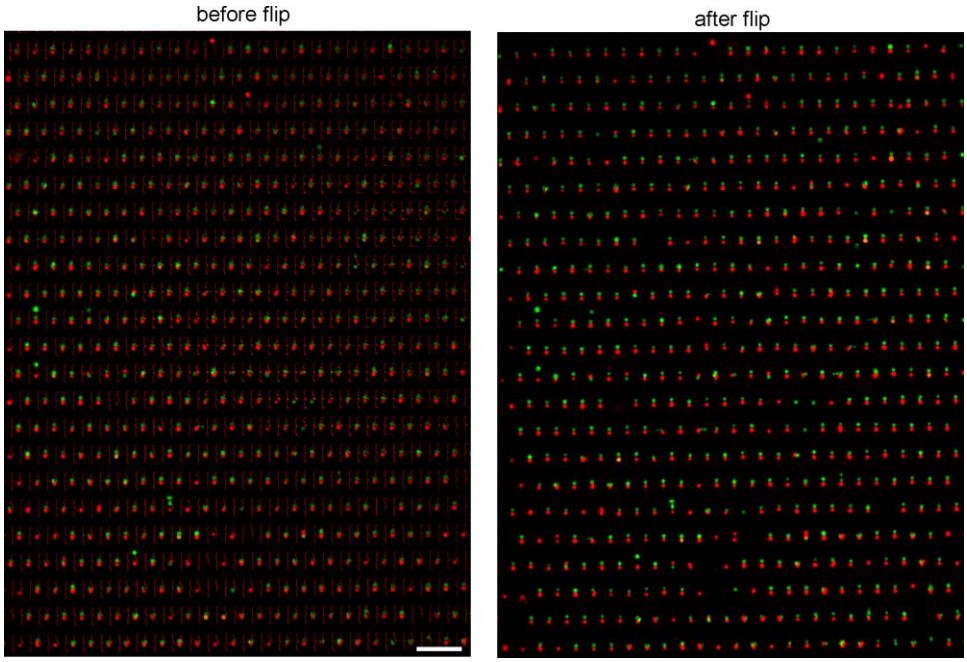

Figure S10. Preservation of cell pairs after device flipping during cell recovery procedure Representative image of the cell pairs before and after flipping the devices (cell pair loss < 1%, n=5). Scale bar 200 μm.

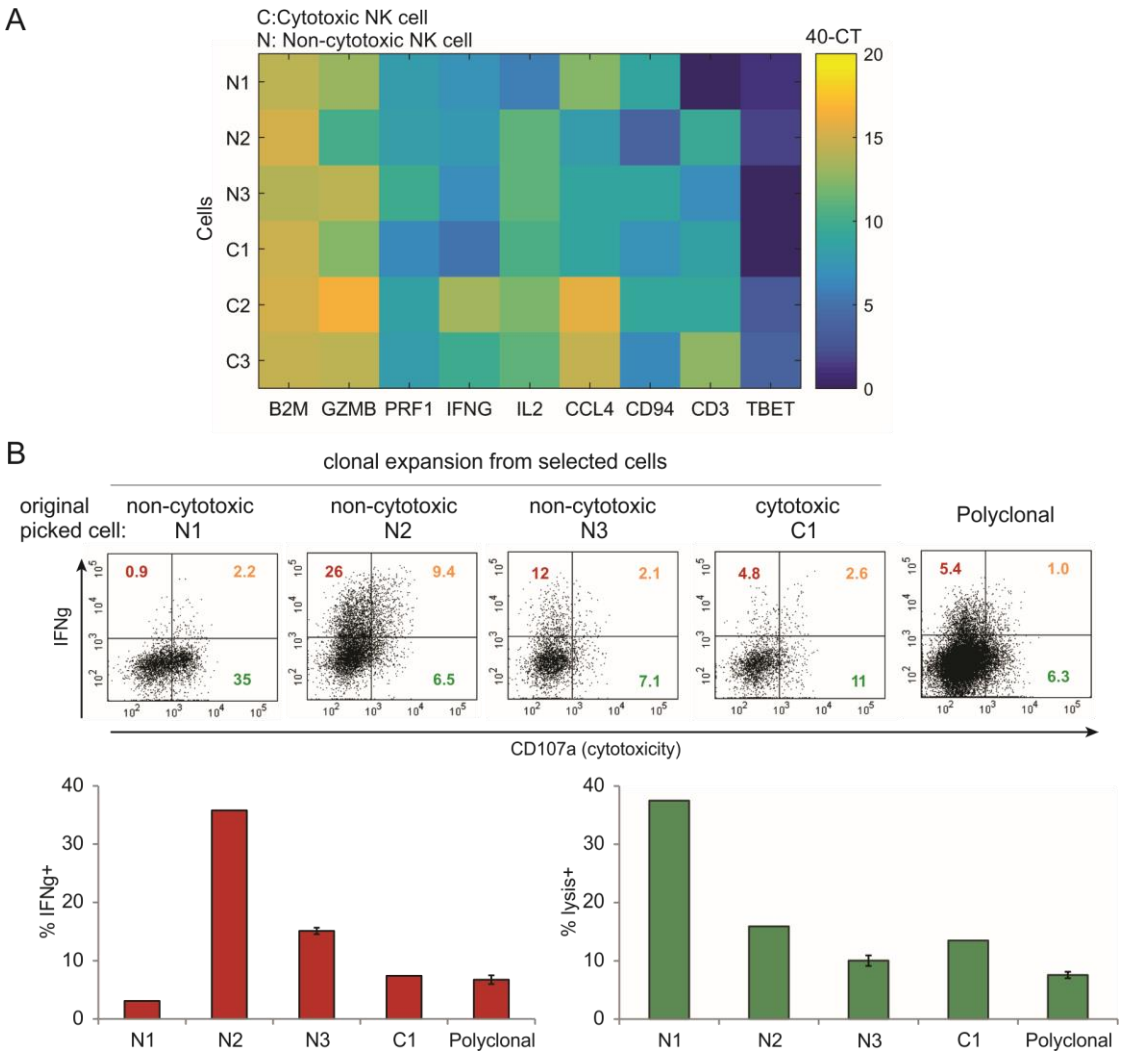

Figure S11: Downstream analysis of retrieved single cells. (A) Demonstrative gene expression analysis of NK cells recovered after on-chip cytotoxicity assay. After assessing cytotoxicity responses and recording the address positions of cytotoxic NK cells, 9 cytotoxic and 8 non-cytotoxic NK cells were arbitrarily recovered, and whole-transcriptome amplification and cDNA preparation were performed using Smart-seq2 protocol. Successful cDNA yields were obtained from 3 cytotoxic and 3 non-cytotoxic cells, which were then analyzed for several immune-cell related genes to showcase the feasibility of the overall workflow. (B) Demonstration of clonal expansion of recovered single NK cells and functional characterization of their clones. Following a cytotoxicity assay between NK and tumor cells on the chip, 11 cytotoxic and 8 non-cytotoxic NK cells were arbitrarily recovered for off-chip culture. 1 of the cytotoxic cells and 3 of the non-cytotoxic cells survived the subsequent expansion over ~2 months' period, reaching sufficient numbers to run in vitro assays (single cells expanded up to ~10^6 cells). Functional profiles (cytotoxicity and IFN-γ production) of these single-cell clones were then assessed in bulk assays upon co-culture with K562 cells. While the cytotoxic clone (C1) and one of the non-cytotoxic clones (N3) responded very similar to polyclonal population, the other two non-cytotoxic clones, N1 and N2, showed higher cytotoxic activity and IFNγ production respectively compared to polyclonal population, suggestive of heterogeneous clonal expansion patterns more complex than that can be presumed from the original founder cell.

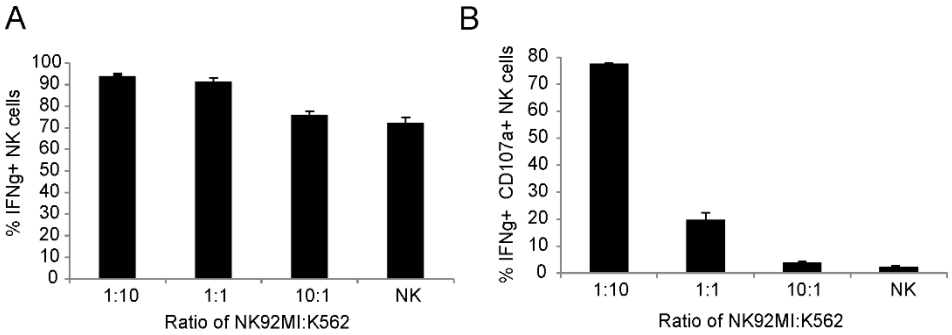

Figure S12. Measurement of IFN-γ production and cytotoxicity in cytokine primed NK92MI cells co-cultured with K562 cells in bulk assays. (A) Percentage of IFN-γ producing cells at different target:effector ratios. (B) Percentage of cells exhibiting cytotoxicity (as determined indirectly by CD107a marker expression) at different target:effector ratios (right panel). Results display expected trends with increasing target:effector ratios, and percentages are similar to that obtained via microfluidic assays. Results are representative of 3 independent experiments.

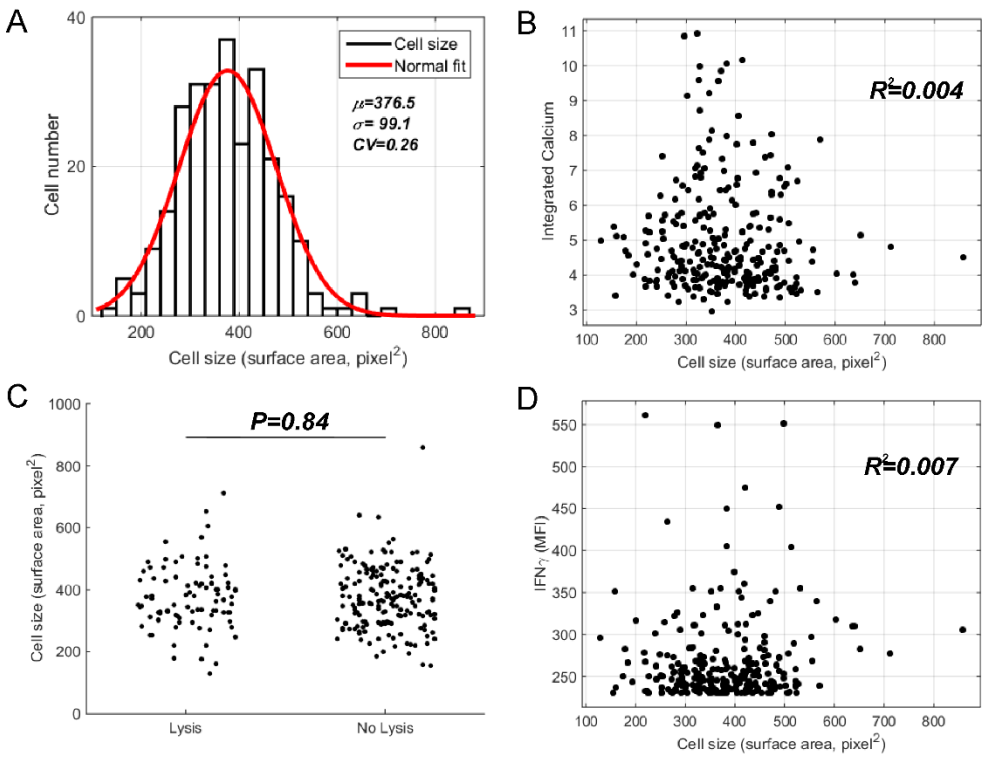

Figure S13: Influence of cell size variation on cellular responses. (A) Cell size distribution of NK92MI cells estimated based on cell surface area. (B) Integrated calcium responses plotted against cell size. Coefficient of determination for linear fit, R^2=0.004. (C) Comparison of cell size between cytolytic and non-cytolytic cells (Student's t-test, *P*=0.84). (D) Interferon-gamma responses plotted against cell size. Coefficient of determination for linear correlation, R^2=0.007. Results from same experiment as shown in Figure 3 in the main text. Representative of 3 independent experiments.

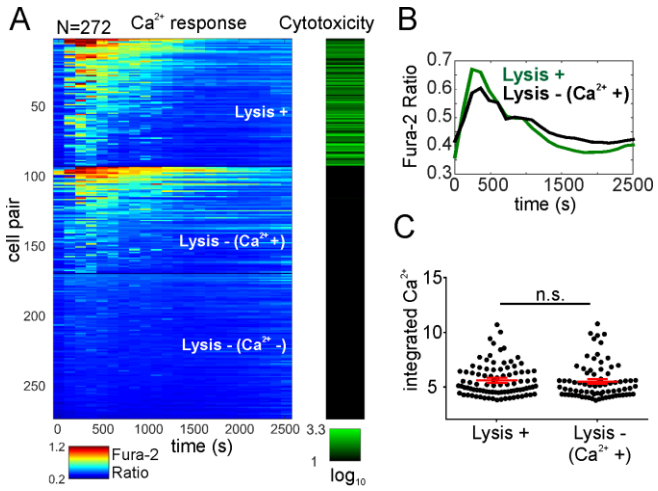

Figure S14: Relationship between Ca^{2+} response and cytotoxic activity of cytokine primed (IL-12, IL-18) NK92MI cells interacting with K562 cells. (**A**) Clustering of Ca^{2+} responses of NK92MI cells based on cytotoxicity responses: 'Lysis +', 'Lysis – (Ca^{2+} +)' and 'Lysis – (Ca^{2+} -)'. Within each group, cells are ordered based on the integrated Ca^{2+} levels. Each cytolytic NK cell displays an associated Ca^{2+} elevation. Ca^{2+} responses are also observable in some of the non-cytolytic cells. Calcium dynamics and cytotoxicity are displayed in jet and red colormaps respectively. Range for each colormap displayed below corresponding colormap (N= 272). (**B**) Comparison of average Ca^{2+} traces of the 'Lysis +' and 'Lysis – (Ca^{2+} +)' groups. (**C**) Comparison of single-cell integrated Ca^{2+} levels of the 'Lysis +' and 'Lysis – (Ca^{2+} +)' groups. Each dot represents a single-cell data. Solid red lines represent mean ± s.e.m. of corresponding data points. n.s., not significant, Mann-Whitney test. (**A-C**) Results are representative of 7 independent experiments.

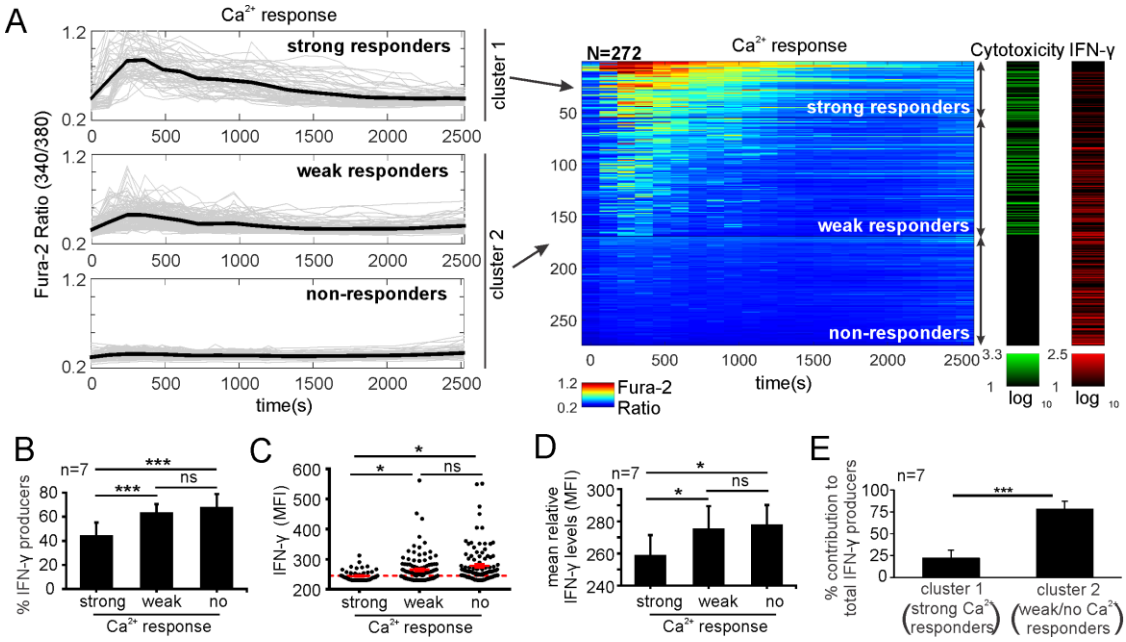

Figure S15. Clustering analysis of Ca^{2+} response dynamics of NK92MI cells (corresponding to Figure 3B in main text). (A) Unsupervised k-means clustering classified responses into two clusters based on sqEuclidean as distance measure. Optimal number of clusters were determined based on average Silhoutte scores. Two clusters identified, and Cluster 2 was further separated into two sub-clusters based on presence of any significant Ca^{2+} activity. Resultant clusters were named as strong responders (Cluster 1), weak responders and non-responders based on the integrated Ca^{2+} levels. Time plots of Ca^{2+} responses shown to the left. t=0 marks the initiation of interaction. Each grey trace represents the response of a single NK92MI cell. Black traces represent the average responses. Corresponding heatmaps of Ca^{2+} responses and associated colormaps for cytotoxicity and IFN-γ production shown to the right. Cluster 1 and 2 are indicated using black double-sided arrows. N represents the number of cells analyzed. Range for each colormap displayed below corresponding colormap. (B) Comparison of percentages of IFN-γ producing cells between strong, weak and non- Ca^{2+} responders. ***$P < 0.001$, one-way ANOVA with Tukey's post-test. (C) Comparison of relative IFN-γ levels (MFI) between IFN-γ producing strong and weak Ca^{2+} responders. Each dot represents a single-cell data, only IFN-γ positive events are shown. Dashed red line indicate the threshold for positive cytokine production events. Solid red lines represent mean ± s.e.m. of corresponding data points. *$P < 0.05$., Mann-Whitney test. (D) Comparison of mean relative IFN-γ levels between strong and weak Ca^{2+} responders. * $P < 0.05$, one-way ANOVA with Tukey's post-test. (E) Comparison of percentage contribution to total IFN-γ producing cells from strong and weak Ca^{2+} responders. ***$P < 0.001$, Student's t test. (A, C) Results are representative of 7 independent experiments. (B, D, E) Results are from 7 independent experiments.

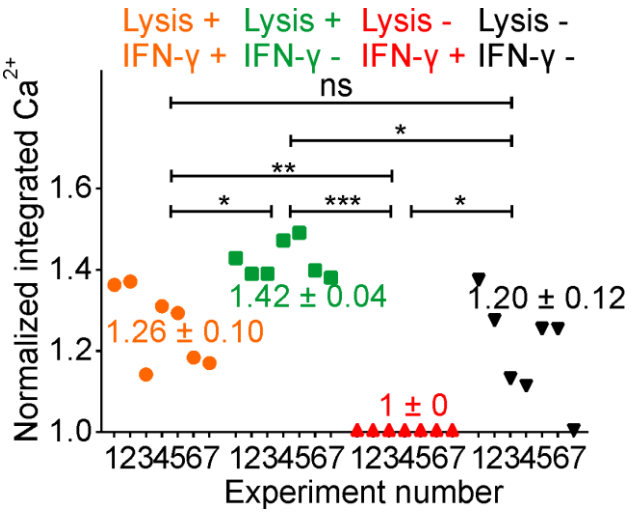

Figure S16. Comparison of the average integrated Ca^{2+} levels among different functional groups. Symbols represent the average level in corresponding experiments and are color-coded for indicating functional groups. Levels were normalized with the corresponding average integrated Ca^{2+} level (lowest) from 'Lysis-IFN-γ' subgroup to compare data among different experiments. Normalized averages of the experiments, mean ± sd, for each functional group shown next to corresponding data points. *P < 0.05, **P < 0.01, ***P < 0.001, n.s. not significant, repeated-measures one-way ANOVA with Tukey's post-test.

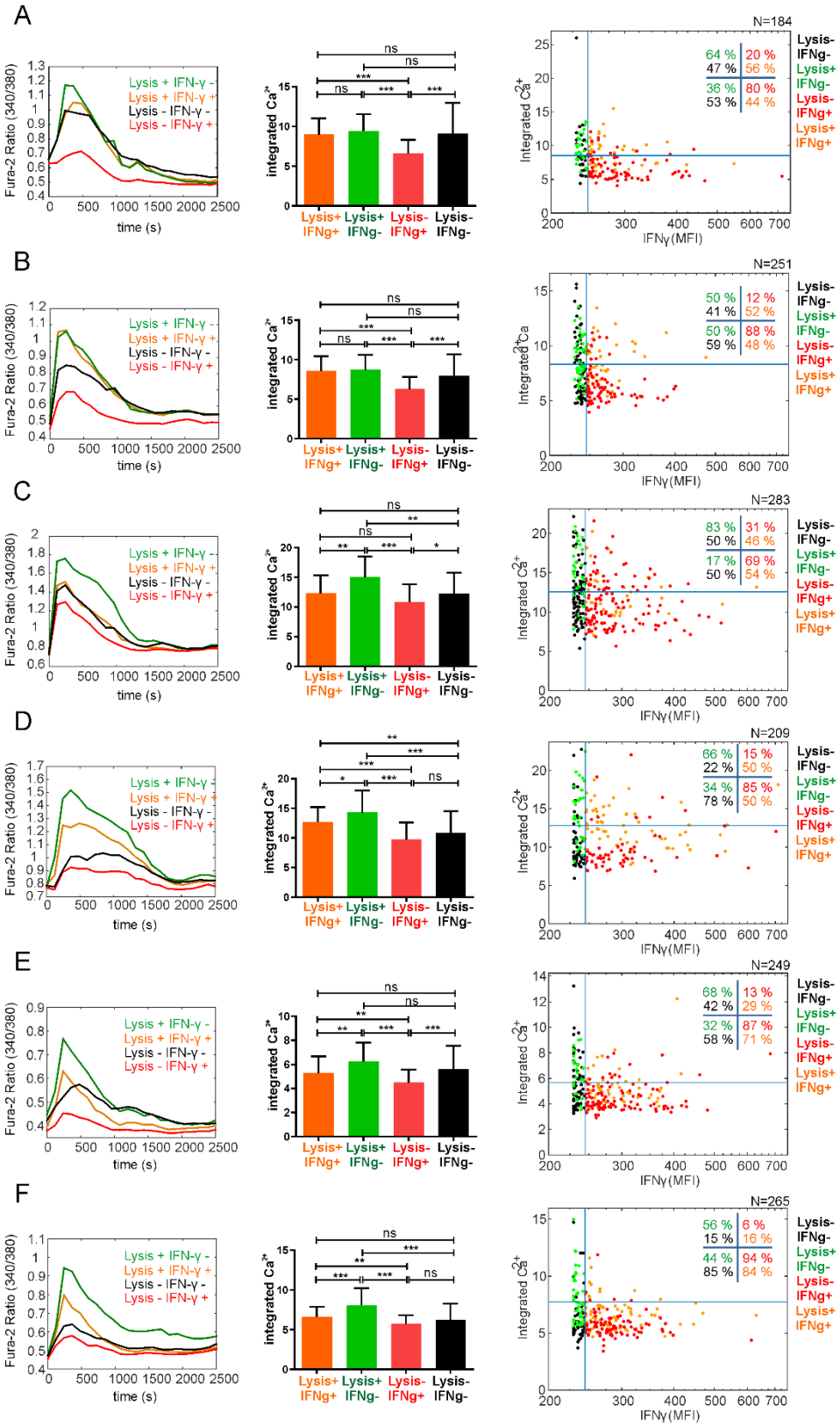

Figure S17. Comparison of Ca^{2+} responses of cytokine primed (IL-12, IL-18) NK92MI cells within different effector response groups (independent repeat experiments for Figure 5 in main text). (A-F)

Each panel represents data from a single independent experiment. Comparison of average Ca^{2+} traces of the functional groups (shown to the left in each panel). Comparison of integrated Ca^{2+} levels among the functional groups (shown in the middle in each panel). Each color-coded column represents a particular functional group. (*P < 0.05, **P < 0.01, ***P < 0.001, n.s. not significant, one-way ANOVA with Tukey's post-test). Scatter plots of integrated Ca^{2+} and relative IFN-γ levels (shown to the right in each panel). Each dot represents a single-cell data, and is color-coded indicating the functional group. Blue lines indicate gating thresholds. Threshold separating the cluster 1 (strong responders) and cluster 2 (weak and/or non- Ca^{2+} responders) was determined based on clustering analysis of each experiment. IFN-γ threshold was determined using unstimulated NK92MI cells as controls. Numbers indicate the percentages of cells within cluster 1 (strong responders) and cluster 2(weak and/or non- responders) in each functional group.

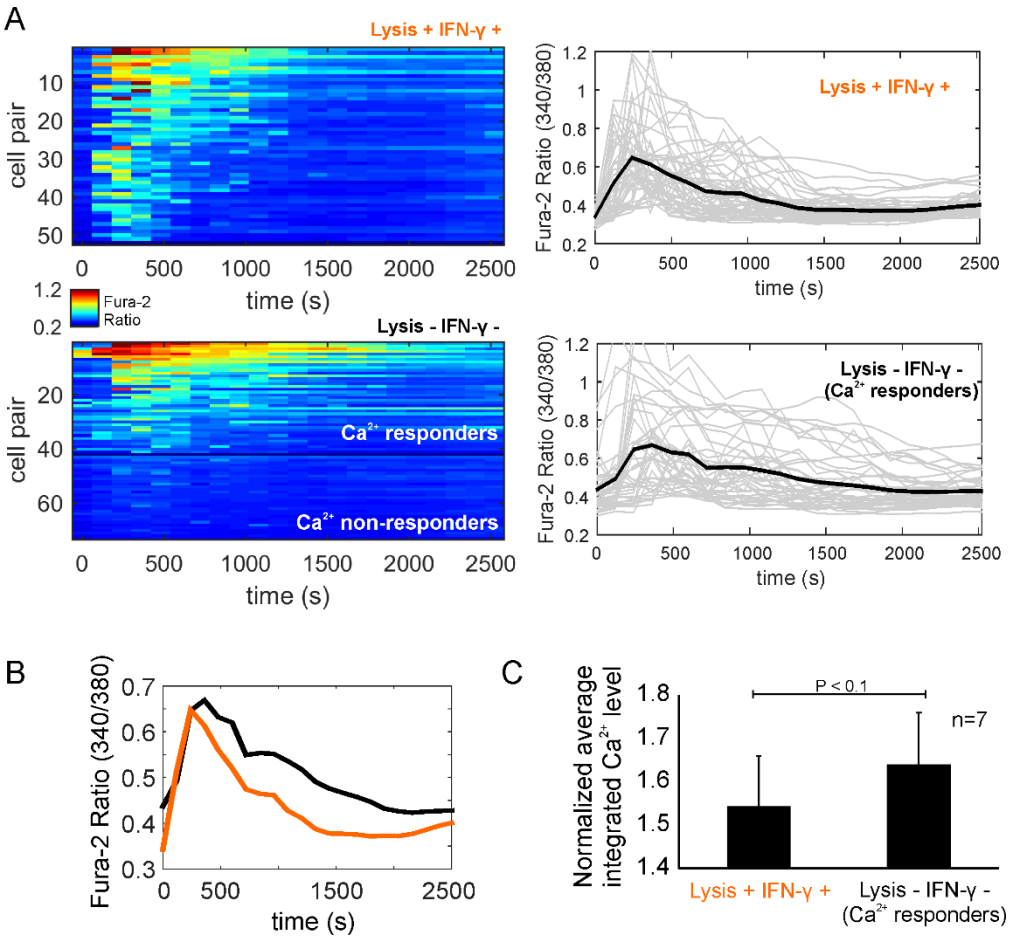

Figure S18. Comparison of Ca^{2+} responses in 'Lysis + IFN-γ +' and 'Lysis - IFN-γ -' subgroups. (A) Ca^{2+} responses (replicated from Figure 5 in main text) were clustered into Ca^{2+} responders and non-responders. While all cells show Ca^{2+} elevation within 'Lysis + IFN-γ +' subgroup, only ~55 % of the cells within 'Lysis - IFN-γ -' subgroup exhibit noticeable Ca^{2+} responses. (B) Comparison of average Ca^{2+} traces between the 'Lysis + IFN-γ +' subgroup and the responding population of 'Lysis - IFN-γ -' subgroup. The responding cells from 'Lysis - IFN-γ -' exhibit higher Ca^{2+} responses than 'Lysis + IFN-γ +' subgroup. (A, B) Results are representative of 7 independent experiments. (C) Comparison of average integrated Ca^{2+} levels between the Ca^{2+} responding populations of 'Lysis + IFN-γ +' and 'Lysis - IFN-γ -' subgroups. Results are from 7 independent experiments. (B) and (C) show that responding cells of 'Lysis - IFN-γ -' display higher Ca^{2+} responses than the 'Lysis + IFN-γ +' subgroup, despite the similar average waveforms when non-responding cells are included (Figure 5B in main text).